

# PROCEEDINGS OF SPIE

[SPIDigitalLibrary.org/conference-proceedings-of-spie](https://spiedigitallibrary.org/conference-proceedings-of-spie)

## Phase A AO system design and performance for MOSAIC at the ELT

Timothy Morris, Alastair Basden, Ariadna Calcines-Rosario, Kjetil Dohlen, Cornelis Dubbeldam, et al.

Timothy Morris, Alastair Basden, Ariadna Calcines-Rosario, Kjetil Dohlen, Cornelis Dubbeldam, Kacem El Hadi, Ewan Fitzsimons, Thierry Fusco, Éric Gendron, François Hammer, Pascal Jagourel, David Jenkins, Carine Morel, Simon Morris, Gérard Rousset, Matthew Townson, Pascal Vola, Edward Younger, "Phase A AO system design and performance for MOSAIC at the ELT," Proc. SPIE 10703, Adaptive Optics Systems VI, 1070316 (13 July 2018); doi: 10.1117/12.2313562

**SPIE.**

Event: SPIE Astronomical Telescopes + Instrumentation, 2018, Austin, Texas, United States

# Phase A AO system design and performance for MOSAIC at the ELT

Timothy Morris<sup>\*a</sup>, Alastair Basden<sup>a</sup>, Ariadna Calcines-Rosario<sup>a</sup>, Kjetil Dohlen<sup>b</sup>, Cornelis Dubbeldam<sup>a</sup>, Kacem El Hadi<sup>b</sup>, Ewan Fitzsimons<sup>c</sup>, Thierry Fusco<sup>b,d</sup>, Éric Gendron<sup>e</sup>, François Hammer<sup>f</sup>, Pascal Jagourel<sup>f</sup>, David Jenkins<sup>a</sup>, Carine Morel<sup>e</sup>, Simon Morris<sup>a</sup>, Gérard Rousset<sup>e</sup>, Matthew Townson<sup>a</sup>, Pascal Vola<sup>b</sup>, Edward Younger<sup>a</sup>

<sup>a</sup>Centre for Advanced Instrumentation, Durham University, Durham, DH1 3LE, UK; <sup>b</sup>Aix Marseille Université-CNRS, LAM, Pôle de l'Étoile Site de Château-Gombert, 38 rue F. Joliot-Curie, 13388 Marseille Cedex 13, France; <sup>c</sup>UK Astronomy Technology Centre, Science and Technology Facilities Council, Royal Observatory Edinburgh, Blackford Hill, Edinburgh, EH9 3HJ, United Kingdom; <sup>d</sup>ONERA, the French Aerospace Lab, F-92322 Châtillon, France; LESIA, Observatoire de Paris, Université PSL, CNRS, Sorbonne Université, Univ. Paris Diderot, Sorbonne Paris Cité, 5 place Jules Janssen, 92195 Meudon, France; <sup>f</sup>GEPI, Observatoire de Paris, PSL university, CNRS, 5 Place Jules Janssen, 92195 Meudon, France

## ABSTRACT

MOSAIC is a mixed-mode multiple object spectrograph planned for the ELT that uses a tiled focal plane to support a variety of observing modes. The MOSAIC AO system uses 4 LGS WFS and up to 4 NGS WFS positioned anywhere within the full 10 arcminute ELT field of view to control either the ELT M4/5 alone for GLAO operation feeding up to 200 targets in the focal plane, or M4/5 in conjunction with 10 open-loop DMs for MOAO correction. In this paper we present the overall design and performance of the MOSAIC GLAO and MOAO systems.

**Keywords:** Adaptive Optics, Laser Guide Star, Natural Guide Star, Multiple Object Adaptive Optics, Ground Layer Adaptive Optics, Wavefront Tomography, Multiple Object Spectroscopy

## 1. INTRODUCTION

MOSAIC<sup>[1]</sup> is a mixed-mode multiple object spectrograph planned for the ELT that has been designed to address the requirements of a broad astronomy user base by covering a large range of potential astronomical science cases<sup>[2]</sup>. MOSAIC uses a tiled focal plane concept capable of deploying small IFUs directly within the focal plane or pickoff mirrors to feed light into larger IFUs or wave front sensors situated at the field edge. Light from each of these systems is sent via optical fiber to one of 5 visible or 5 near-infrared spectrographs for analysis. MOSAIC is the only instrument planned for the ELT that makes use of the entire 10 arcminute field of view afforded by the telescope. The tiled focal plane supports four operating modes that must in turn drive AO architecture and requirements:

- High-Multiplex Mode (HMM) observes a large number of targets using GLAO provided by the ELT M4/5 system and the MOSAIC LGS and NGS WFS. This mode is further subdivided into HMM-VIS (200 objects between 450-1000nm) and HMM-NIR (100 objects and 100 calibration sky fibers between 1000-1800nm)
- High-Definition Mode (HDM) uses larger IFUs situated around the edge of the focal plane to target up to 10 objects within a 7.5 arcminute diameter field between 1000-1800nm. This mode using MOAO correction to concentrate >25% ensquared energy in the H-band onto 2x2 spatial resolving elements each of 80mas in diameter.
- The final operating mode provides 10 visible wavelength (400-800nm) mini-IFUs with a moderate spatial resolution of 0.3 arcseconds across a 2 arcsecond field.

These must operate across a field of view with area at least 40 square arcminutes, with a goal of 80 square arcminutes. This latter goal corresponds to the full Ø10 diameter FOV of the ELT. A more detailed description of the MOSAIC conceptual (Phase A) design can be found elsewhere within these proceedings. Here we present the AO system conceptual design and present initial performance estimates based on results from several independent Monte-Carlo and analytical

simulations. We detail the opto-mechanical designs of the primary AO-related components (LGS WFS, NGS WFS and Deformable Mirror relays). We also describe the AO real-time control system implementation capable of running the system at the required update rate of 250Hz using architecture developed under the UK ELT program and optimized under the H2020 GreenFlash project<sup>[3]</sup>. This real-time control system architecture covers both the low-latency 'hard' real time control pipeline and the supervisor required to monitor and optimize AO system performance. In addition to describing system GLAO and MOAO performance, we present the calibration scheme, analysis of the impact of a conjugated adaptive secondary on both GLAO and MOAO performance, and errors associated with flexure compensation within the large rotating structure.

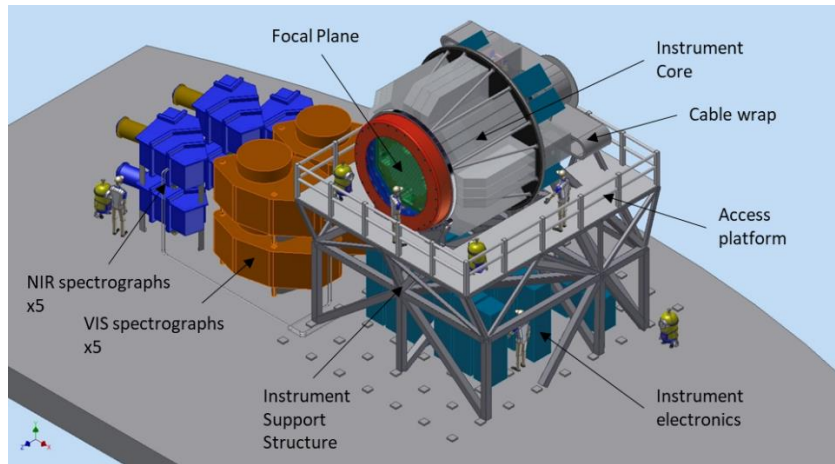


Figure 1 MOSAIC instrument model installed on the ELT Nasmyth 'B' platform showing major instrument subsystems

### 1.1 Adaptive Optics architecture

A simplified model of the AO architecture including basic optical path and data flows is shown in Figure 2. Wavefront aberrations across the field of view of MOSAIC are analyzed using data from four 74x74 sub-aperture Shack-Hartmann LGS WFS and up to four 74x74 sub-aperture NGS WFS distributed anywhere within the Ø10 diameter field, except for areas required for the LGS. The real-time control system calculates ELT M4 and the ten open-loop MOAO deformable mirror shapes at a primary loop rate of 250Hz as well as providing all the monitoring and optimization functions required to maintain AO system stability.

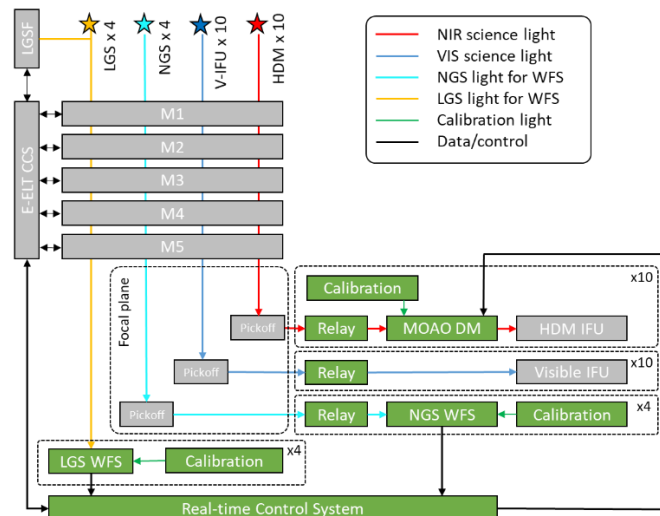


Figure 2 Schematic overview of AO architecture showing light path, principal internal AO-related subsystems (in green) and data flow. External telescope and MOSAIC modules interfacing with the AO system are shown in grey.

## 2. SYSTEM DESIGN

### 2.1 Focal Plane

The Ø2m diameter focal plane consists of a number of tiles that position HMM fiber or pickoff mirrors that direct light to the edge of the focal plane (see Figure 3). Twenty-four optical relay modules are then distributed around the field periphery. The optical relay modules can accept light from approximately 30% of the tiles in the focal plane with every tile addressable by at least two relay modules. Each relay module transmits an unvignetted 4" field of view with a 1:1 magnification of the focal plane. Either a HDM IFU, V-IFU or NGS WFS can be mounted to the rear of each module. The optical relays feeding the HDM IFUs also contain a 32x32 actuator deformable mirror for MOAO correction.

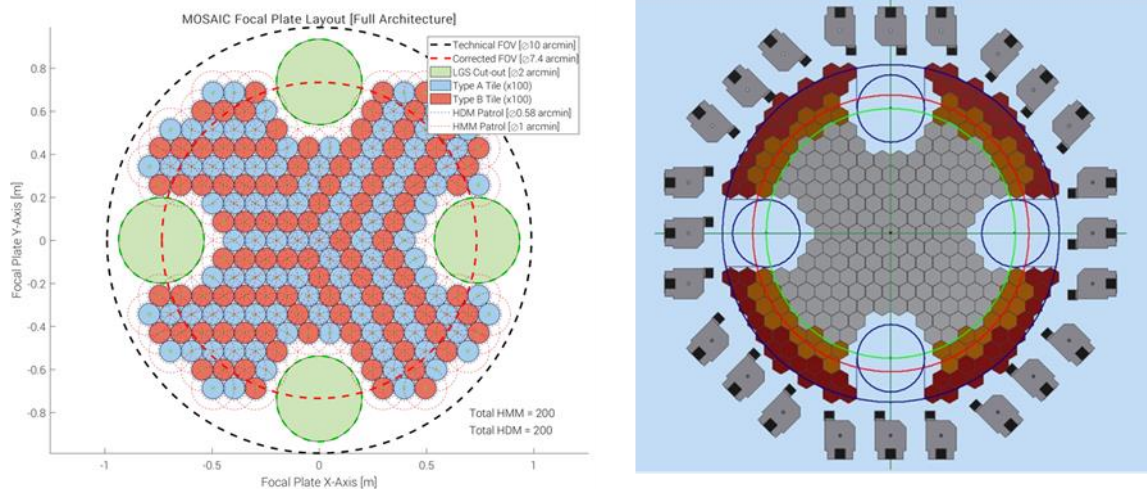


Figure 3 Tiled focal plane showing tile allocation presented for the Phase A/conceptual design (left) and the distribution of the optical relay modules at the focal plane edge (right). The 4 large circular apertures are required to pass the LGS beams to the LGS WFS situated behind the focal plane.

The tile concept was selected as the only concept that can cope with the non-telecentric and curved ELT focal plane whilst meeting the requirements for reconfiguration time and the need to position NGS WFS and MOAO DMs within the field of view.

One of the key AO design parameters related to the location and number of the LGS within the MOSAIC field of view. This defined not only the overall AO performance levels in terms of global tomography error, but also defined much of the full MOSAIC architecture. The selected LGS configuration with 4 LGS equidistantly spaced around a circle of Ø7.4 arcminutes and the LGS WFS situated behind the focal plane was selected as the optimal configuration for the instrument based on an extensive system-level tradeoff. This by definition means that the LGS will track the sky, rather than tracking the pupil/M4 as with all other proposed ELT instruments. Other than AO performance, described further in section 3, the primary drivers for this choice were:

- WFS co-alignment. In the configuration the LGS track the sky, and therefore remain fixed with respect to both science targets and NGS WFS during an observation. This greatly reduces the computational load related to the calculation of the tomographic wavefront reconstructor that is one of the main dimensioning operations within the real-time control system
- LGS Path length. Obviously placing the LGS behind the focal plane takes up much of the additional path length required for the finite-distance LGS. This allows a modest reduction in LGS optics diameter and thus LGS WFS mass.
- Focal plane access. Placing the LGS WFS behind the focal plane allows much better access to the focal plane (e.g. for tile replacement) and increases the space allowed for the pickoff system and pre-focal plane science calibration.

- Mass reduction. Having the LGS asterism track the sky rather than the pupil removes the requirement for an additional bearing to allow differential rotation between the sky-tracking focal plane and the pupil tracking LGS WFS.
- Increased field of view. If the LGS rotate with respect to the pupil, the rotation of the LGS on the focal plane will vignette the edge of the field during observation. This limits the available field for science and suitably bright natural guide stars to this inner region of 5 arcminutes diameter. This can have a severe impact both on sky coverage as it halves the available area to find bright NGS, and also limits survey speeds as additional pointings are required to cover the sample of cosmological fields used as test targets.

The drawback of this approach is that perspective elongation pattern is no longer fixed on each LGS, requiring LGS reference slopes updates during observation. The LGS WFS sub-apertures used for tomographic reconstruction may also vary during the course of an observation as the pattern of overlapping highly elongated SH spots varies. This affects approximately 15-20% of all LGS WFS sub-apertures dependent on the sodium layer depth. Both of these effects can be accounted for within the real-time control system. Finally, only a limited (100 degrees for the current LGS asterism) sky rotation can be tolerated before LGS fratricide is observed. This has a slight impact on observational efficiency for near zenith observations as LGS must be reacquired.

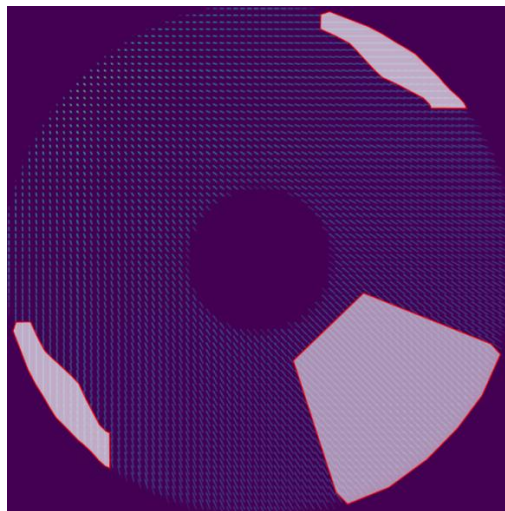


Figure 4 LGS WFS sub-apertures (indicated by white areas) affected by overlapping elongated spots for a typical 15km thick sodium layer assuming no field stop and software-defined elliptical pupil masks are implemented.

## 2.2 LGS WFS

The four LGS WFS modules are mounted behind the focal plane as shown in Each module contains means for focusing the laser guide star to its apparent distance ranging from 90 to 180km, corresponding to a median-altitude sodium layer of 90km seen at altitudes ranging from zenith down to 30 degrees, consisting of a dihedral mirror mounted on a linear translation stage. It also includes a mechanism for correction of pupil motion to within 0.1% of the pupil diameter, consisting of a dual-axis rotation stage. These two mechanisms are the only moving elements within the LWM, leaving all powered optics fixed. These are field optics at the entrance of the system, creating an intermediate pupil image, and camera optics, creating a telecentric, fixed focal ratio, intermediate image. Each of these optical systems consist of two aspheric lenses located upstream of the focusing stage. These lenses are fairly large in order to accommodate the large range of apparent object distances. Downstream of the focusing stage, following the pupil stabilization mechanism, there are smaller optics for projecting the pupil onto the micro-lens array and relay optics projecting the Shack-Hartmann spots onto the detector. The bench is currently considered in the form of a steel honeycomb structure, similar to standard optical breadboards, but if further thermal and structural analysis imposes an aluminum structure this is fully compatible with our design.

The baseline NGSD detector<sup>[4]</sup> does not provide enough pixels to both optimally sample the elongated LGS image and avoid spot truncation/overlap within WFS sub-apertures located at points in the pupil furthest from the LGS launch telescope location. There are several possible mitigations to the issue of LGS spot elongation that have been proposed<sup>[5]</sup>,

and several of these are under active investigation<sup>[6]</sup>. Mitigation of the rotating LGS WFS spot pattern, including the use of alternative detectors will be investigated fully during the next phase of the project.

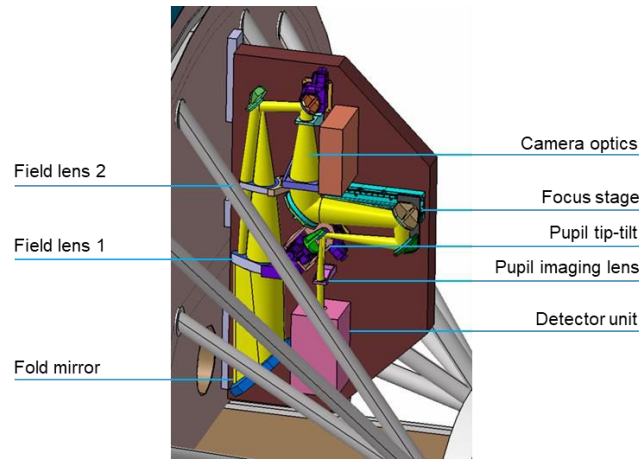


Figure 5 LGS WFS module design mounted to the rear of the MOSAIC focal plane. LGS light enters from the aperture by the fold mirror.

### 2.3 NGS WFS

Four NGS WFS will be mounted directly at the output of four relay modules channels as indicated in Figure 6. The baseline NGS WFS calls for a 74x74 sub-aperture Shack-Hartmann WFS with 10x10 pixels and a 0.4 arcsecond pixel scale that can operate at a frame rate of 250Hz. Both the NGSD, developed by ESO<sup>[4]</sup>, and several commercially available sCMOS detectors meet these requirements, however the lower read noise of the sCMOS device will result in better performance. For the highest sky coverage, replacing the NGSD or sCMOS devices with an EMCCD device that operates at a lower spatial sampling and/or frame rate<sup>[10]</sup> is an option that will be investigated during the next phase of the project.

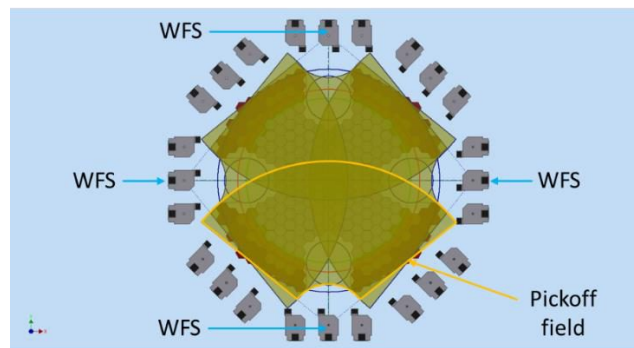


Figure 6 Distribution of NGS WFS channels around the focal plane showing the overlapping pickoff field for each NGS WFS.

### 2.4 Optical Relay

The twenty four optical relay modules within the system each re-image a 4 arcsecond diameter region of the ELT focal plane and provide an accessible output focal plane at which to place IFUs and NGS WFSs. The components within each module are as follows:

- **Beam Steering Mirror (BSM).** This is a flat steering mirror that accepts a reflected beam from a subset of pickoff mirrors placed within the field and directs light into the trombone system.
- **The Trombone** comprises two mirrors mounted on a linear translation stage that ensures the optical path length between the pickoff mirror in the telescope focal plane and first powered mirror within the relay remains constant. The size of trombone mirrors and range of the linear stage has been selected such that it maximizes the area of the focal plane that can be addressed by any individual relay channel.

- Pupil Imaging Mirror (PIM). This mirror creates a pupil conjugated plane of 72mm in diameter within the relay where the deformable mirror can be positioned.
- Pupil Mirror (PM). This is included within this concept as a location for the MOAO DM, pupil mask/cold stop, or tip-tilt mirror.
- Imaging Mirror (IM). The imaging mirror creates the output focal plane at a fixed location with respect to the ICOS. The output IM here has been designed to recreate the ELT f-ratio of 17.7
- Pupil Lens (PL). This lens is placed just before the output focal plane to constrain telecentricity at the output focus.

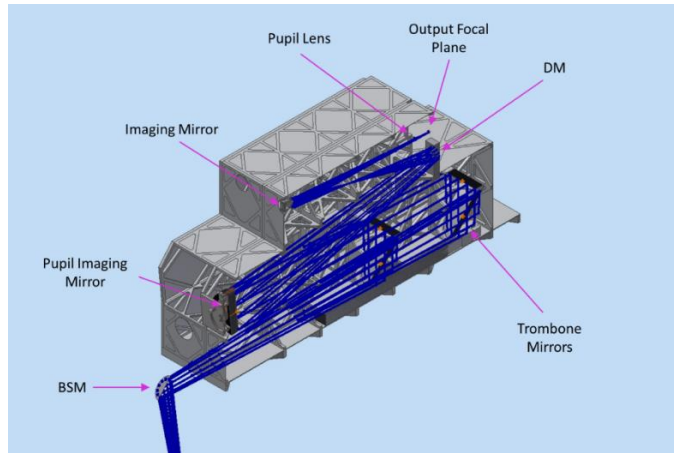


Figure 7 Optical components and internal mechanical structure of optical relay module arranged in a block of three relay channels.

Each optical relay module rotates with the field, therefore is susceptible to flexure that can affect image quality, output PSF location and pupil alignment.

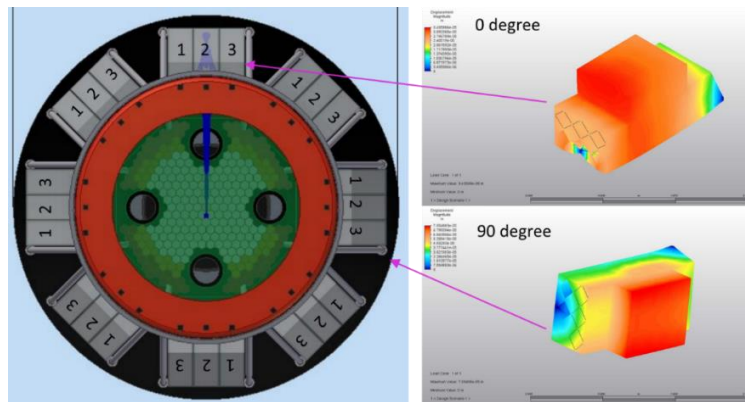


Figure 8 Flexure within a block of three optical relay modules through a 90 degree rotation of the instrument core.

Analysis of flexure within each of the channels was assessed at several rotation angles and suggests both pupil motion and PSF position will require active compensation:

- A change in wavefront error of 30-40nm RMS
- Pupil motion at the MOAO DM of up to 10.2% of actuator pitch
- PSF motion at the IFU/bundle of up to 1.2"
- Pupil shift at IFU/fiber injection of 0.06%

## 2.5 AO Calibration

Within each relay there are two focal planes, the output focal plane for the IFU/WFS, and an intermediate focal plane. Access to the intermediate focal plane is restricted as it lies within the ORM structure and this focal plane also exhibits poor image quality, limiting its use as a wavefront/calibration reference. The calibration unit is designed to place a source at a picked-off focal plane conjugate to the output focal plane. Two potential locations for the calibration unit are highlighted in Figure 9. The location (green or blue) of the unit will be dependent on the size of the calibration systems required. Requirements on the sources within the calibration module are defined within section 9.1.

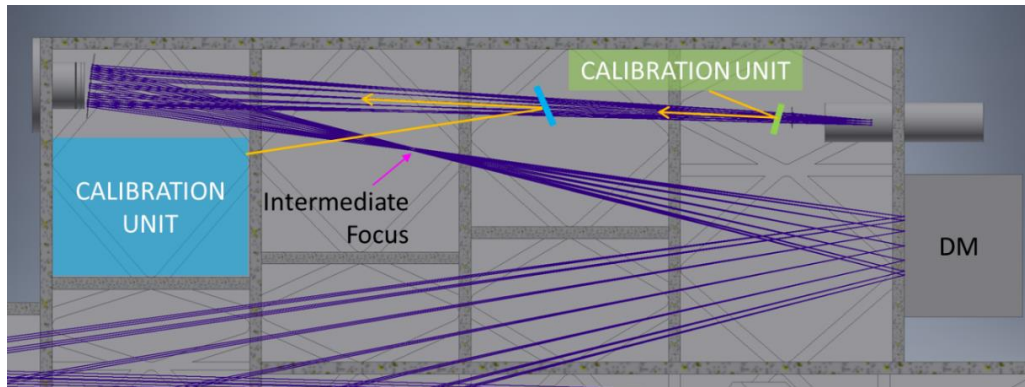


Figure 9 Potential calibration unit locations within optical relay modules that can be used to back-illuminate the deformable mirror and the optical trombone system.

The calibration module is a deployable system within each optical relay that is used primarily to provide back-propagation reference source(s) for AO calibration. By pointing two relay channels towards one another using their respective beam steering mirrors, the calibration units inside one channel can be used to calibrate the other (Figure 10). The back-illumination sources allow several critical functions to calibrate the AO system and re-a:

- Measurement of MOAO DM interaction matrices.
- Analysis of non-common path errors within relay channels (during instrument rotation)
- Analysis of pupil motion within relay channels (during instrument rotation)
- Closed-loop MOAO DM testing
- PSF optimization algorithms within HDM and VIFU channels.

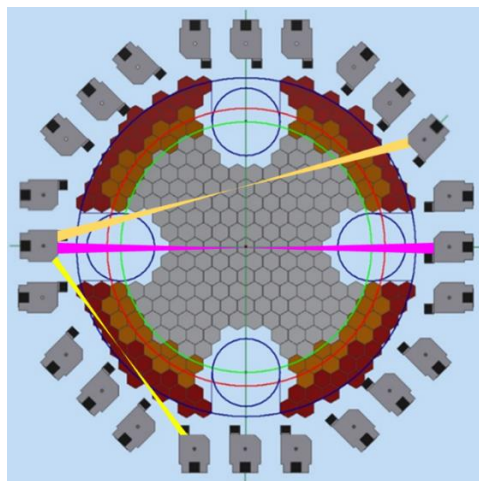


Figure 10 Relay module cross-calibration with multiple channels directed towards a WFS channel for flexure and AO calibration.

Depending upon the precise distribution of HDM channels around the focal plane, each HDM channel should be able to illuminate at least 2 NGS WFS channels. This configuration will be the primary means of MOAO system calibration, however we note that the measured interaction matrices will have to be rotated to match the eventual on-sky configuration. Both the NGS WFS and MOAO DM rotation angle is a function of the POM and BSM rotation angles and will have to be accounted for in the RTCS. LGS WFS will be static and rotationally aligned to one another.

## 2.6 AO Real-time control system

The real-time control system is responsible not only for providing the low-latency WFS pixel processing, tomographic reconstruction and M4/MOAO DM commands, but also all monitoring, status and optimization loops that are required to maintain performance during observations. In addition to this the system must store and process large amounts of telemetry to assist with astronomical data reduction. The MOSAIC RTCS is comprised of four primary components:

- Hard real-time pipeline – low-latency pixel processing, DM shape calculation and interfaces to ELT adaptive systems (M4/5 and LGS TT mirror) and interfaces to instrument DMs.
- Soft real time system – implements non-real-time system control, monitoring, offload and performance monitoring algorithms. Also includes a data storage system.
- Telemetry sub-system – provides control, status, and access to real-time data streams and supervisor algorithms
- Network architecture – low-latency high bandwidth data transport

Many of the interfaces within this system are being defined at the observatory level (such as the telemetry sub-system, WFS-to-RTC data formats and some aspects of the network architecture) and the overall RTC architecture that matches both MOSAIC and observatory required interfaces is shown in Figure 11.

Although MOSAIC contains more actuators than any proposed ELT AO system due to the many MOAO deformable mirrors required, the reduced system frame rate of 250Hz and ability to treat each MOAO channel independently leads to an inherently parallelizable architecture that can be distributed amongst several compute nodes<sup>[7]</sup>. There are several potential hardware architectures that can be used for this pipeline and some have been prototyped through the H2020 GreenFlash<sup>[3]</sup> project for systems of similar dimensions to MOSAIC<sup>[8]</sup>. We therefore believe this pipeline does not require further development work and is currently a low risk. The soft-real time system however will require additional work over the next project phases to minimize the required computing resources particularly for e.g. the generation of the tomographic reconstruction matrices required for each MOAO channel<sup>[9]</sup>.

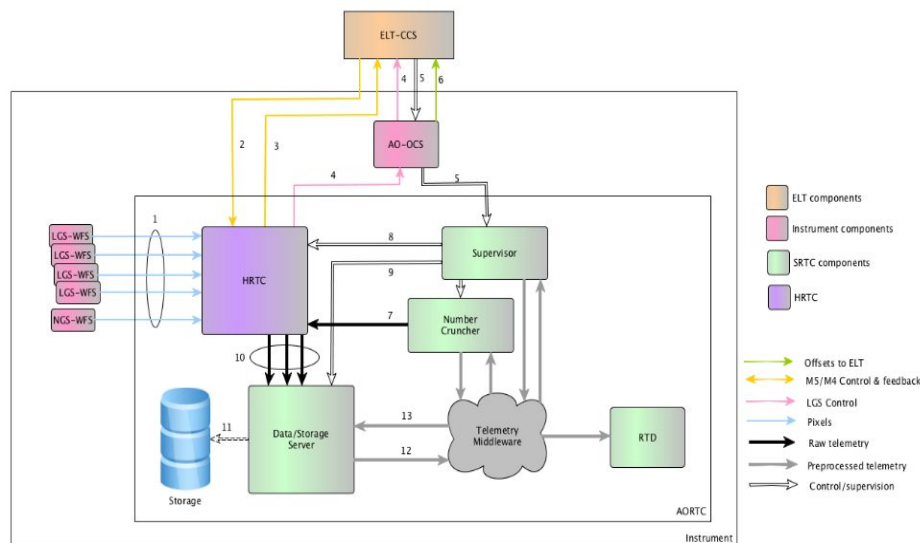


Figure 11 Preliminary MOSAIC RTC architecture diagram showing primary RTC functional modules and data/control flow within the system. Links to MOAO deformable mirrors are not shown.

### 3. AO PERFORMANCE

The AO system design requirements are defined principally by the Ensquared Energy (EE) requirements of 25% at the HDM IFU input operating in MOAO mode. This requirement must be met for at least 10 targets (goal of 20 targets) within a field of 40 arcminutes squared (goal of 80 arcminutes squared). GLAO and MOAO are the only AO techniques currently feasible for providing correction across this field of view<sup>[11]</sup>.

Sky coverage was estimated based on the ability of the system to meet performance requirements whilst observing a set of real asterisms. These were generated from simulated surveys covering real cosmological fields that will be observed with MOSAIC<sup>[12]</sup>. A baseline asterism was selected for performance comparison that provided the median tomographic error for a range of asterisms<sup>[13]</sup>. These asterisms were used for both GLAO and MOAO performance estimates, however it was clear from these studies that to find 3+ sufficiently bright NGS, the full 10 arcminute field of view must be used.

#### 3.1 MOAO

MOSAIC AO performance requirements define very low Strehl ratio correction, therefore an error budget based solely on wavefront error cannot accurately represent system performance without distributing errors terms across a range of low and high-spatial frequency scales. System design was therefore based upon sensitivity analyses of the deviation from a baseline AO architecture. Here we made use of extensive modelling and simulation work undertaken on prior ELT MOAO instrument studies<sup>[10][11][12][13][14][15]</sup> to determine an initial baseline that would exceed our performance goals. The architecture could then be simplified to meet requirements (with both a 2.5% EE and corrected field area contingency to account for non-modelled error terms, such as telescope vibrations) to reduce both AO system cost and mass.

The main scope for reducing overall cost could be realized with a reduction in the number of actuators within the open-loop deformable mirrors, and/or a reduction in the number of wavefront sensors. A summary of the principal pseudo-analytical simulation<sup>[15]</sup> trade-off results is presented in Figure 12 which shows the area of the field that meets a given H-band EE performance for a range of NGS and LGS asterisms and both GLAO and MOAO configurations under median seeing conditions. These baseline conditions have been defined in previous proceedings in this series<sup>[16]</sup> with an  $r_0$  of 15.7cm at a zenith. From these plots we can draw several conclusions:

- GLAO just meets the corrected field area requirement of 40 arcmin<sup>2</sup> with EE>27.5% for both 4 LGS and 6 LGS configurations irrespective of the number of NGS. However, small variations in ground-layer/free-atmosphere turbulence distribution that may not be captured within the 5 defined atmospheres used for this study may invalidate this conclusion as the corrected field area varies.
- An NGS-only MOAO system is a possibility if 5 NGS can be found within the field, however a DM with greater than 32x32 actuators would be required within each MOAO channel to provide some corrected field area margin. Whilst this is a possibility, this can be an expensive solution compared to the inclusion of additional LGS WFS if the number of MOAO channels is large. The increased number of NGS required also has some impact on sky coverage meaning only 75% of the cosmological fields identified could be observed.
- The architecture that minimizes the number of WFS and MOAO DM actuators uses 4 LGS and 3 NGS with 32x32 actuator deformable mirrors within the MOAO channels.

This latter configuration was selected as the baseline for the MOSAIC Phase A study upon which the instrument architecture (principally defined by the focal plane configuration) could be further investigated. Subsystem design tradeoffs within the AO system that did not affect this architecture (such as varying the number of actuators in the MOAO DM, or WFS frame rate) could then be investigated in parallel to the rest of the instrument design and fed into future design iterations. We note that the system design presented here includes 4 NGS WFS rather than the 3 required NGS WFS to ensure that all points in the field can be addressed by at least two WFS.

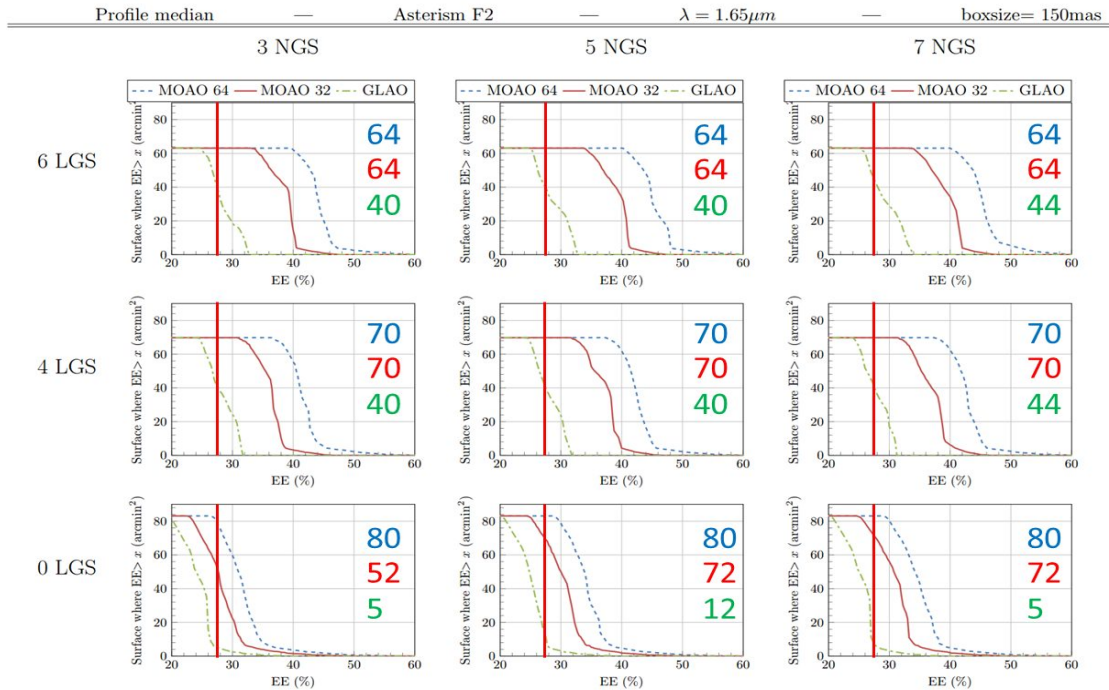


Figure 12 Area of corrected field of view meeting a given ensquared energy for nine WFS configurations covering 3 to 7 NGS and 0 to 6 LGS. For each WFS configuration curves describing the EE vs. corrected field area for GLAO (ELT M4 only) and MOAO with M4 and an additional 32x32 or 64x64 actuator open-loop DM are shown. Numbers in show the corrected field area in arcminutes for MOAO64 (blue), MOAO32 (red) and GLAO (green). Simulations have been performed at a wavelength of 1.65 microns for the ESO 35 layer median atmosphere. The thick red vertical line shows the EE performance requirement (including contingency) of 27.5%.

### 3.2 M4 conjugation

One aspect of the ELT design is that the tilted M4 is conjugated across a range of conjugate altitudes of approximately 530-630m. The inclusion of a conjugated M4 within simulations showed a large effect on wide-field AO performance, as this corresponds to a significant pupil shift (in terms of actuator spacing) as the field angle is varied (see Figure 13).

M4 conjugation degrades both MOAO performance across the field by approximately 5-7% EE compared to the ground conjugated M4 used in early simulations used to define the baseline architecture. It also adds a field dependency to both the GLAO and MOAO correction, however we note that performance and field area requirements are still met with the baseline architecture under median conditions. We also note that this effect does not impact narrow-field LTAO performance but may have a small impact on the performance for wider-field MCAO systems. The full impact of M4 conjugation on MOAO performance will be studied further when the system error budget is developed in the next project phase, however the number of actuators and DM stroke within the MOAO channels can be used to compensate for these field dependent effects and restore corrected field area if required.

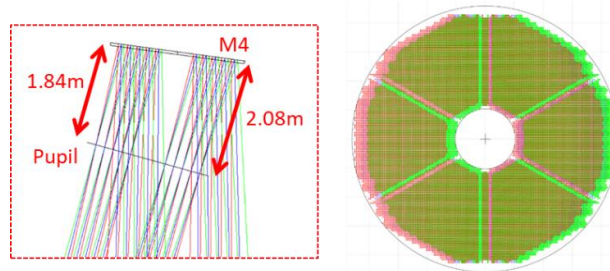


Figure 13 Tilted conjugation of ELT M4 (left) and beam footprint at M4 showing for the +/- 5 arcminute off-axis fields of view.

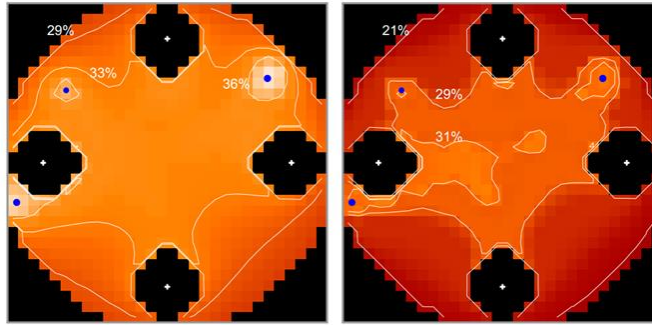


Figure 14 Map of the 10 arcminute diameter ELT field generated using the pseudo-analytic simulation<sup>[15]</sup> showing H-band ensquared energy within 150 milli-arcseconds for a system with 4 LGS (location shown with white dots), 3 NGS (blue dots) for MOSAIC with a 32x32 actuator MOAO DM, and a ground conjugated M4 (left) and a 612m conjugated M4 (right).

### 3.3 GLAO

The GLAO system does not have a formal performance requirement, although we note that the three systems that can be used with GLAO correction are the HMM-VIS (0.8" sampling), HMM-NIR (0.5" sampling) and V-IFU (0.3" sampling). Whilst GLAO can be provided using LGS and NGS, or NGS alone, here we present results showing performance using 4 LGS and 3 NGS. Note that the definition of astronomical seeing has been modified for the ELT<sup>[17]</sup> and does not include an outer scale component, therefore the median seeing of 0.702 arcseconds will correspond to a significantly smaller measured FWHM when observed with the 38m diameter ELT, hence the  $>0.5$  arcsecond FWHM simulated performances indicated within the remainder of this section.

M4 conjugation has an impact on GLAO performance has been calculated using a Fourier domain analytic simulation<sup>[18]</sup> as shown in the two plots below that shown GLAO performance in terms of PSF FWHM as the conjugate altitude of M4 is varied at wavelengths of 600nm (Figure 15) and 1600nm (Figure 16). The 1600nm plot also includes the MOAO-corrected FWHM for comparison. Whilst we note from these plots that the FWHM remains well below the HMM-VIS and HMM-NIR sampling at both wavelengths, significant reduction in FWHM can be observed (even at 600nm) by reducing the diameter of the GLAO corrected field. This can be achieved without modifying the NGS/LGS asterism, but by adapting the reconstructor. This may provide some scope for a reduced-field operating mode during periods of poor seeing, or strong high-altitude turbulence.

Finally we note that the tilted conjugation of M4 has not been explicitly included within these simulations. Looking at the FWHM for the 7.5 arcminute diameter corrected field we can see that varying DM conjugation altitude from 530m to 630m will change the PSF FWHM. This variation will occur across the pupil however, which may result in more complex PSF modelling requirements.

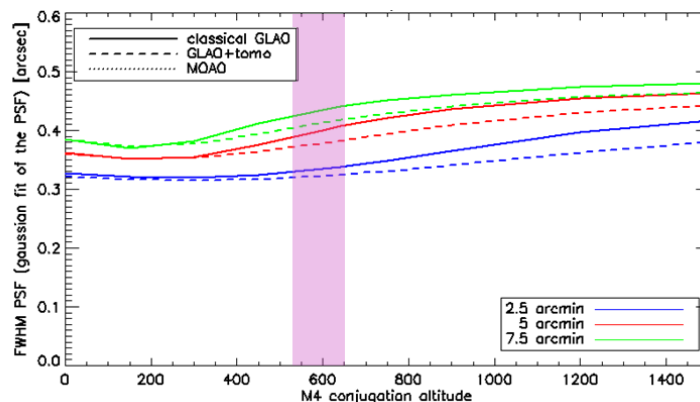


Figure 15 GLAO performance at 600nm vs M4 conjugation altitude. Blue, red and green lines show the field-averaged FWHM for GLAO correction optimized for 2.5 arcminute, 5 arcminute and 7.5 arcminute diameter fields respectively. Dotted lines plot performance with a tomographic GLAO reconstructor, solid lines with a classical averaging GLAO reconstructor. Purple region shows approximate conjugation altitude range of M4.

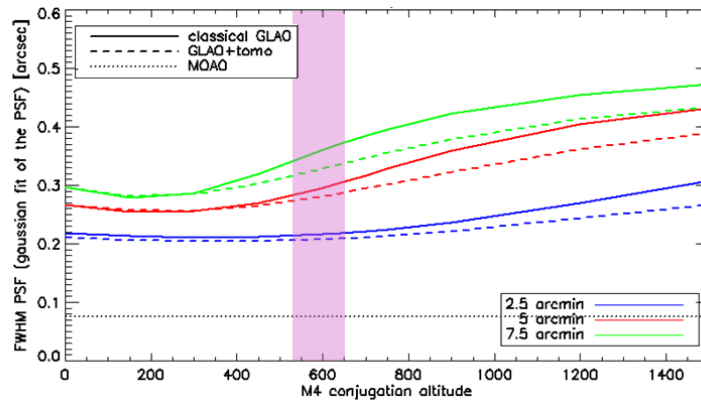


Figure 16 GLAO performance at 1600nm vs M4 conjugation altitude. Blue, red and green lines show the field-averaged FWHM for GLAO correction optimized for 2.5 arcminute, 5 arcminute and 7.5 arcminute diameter fields respectively. Dotted lines plot performance with a tomographic GLAO reconstructor, solid lines with a classical averaging GLAO reconstructor. MOAO performance is shown as dotted black line. Purple region shows approximate conjugation altitude range of M4.

#### 4. CONCLUSIONS

We have presented the architecture and performance of the MOSAIC AO system and summarized the main design studies that were used to select this system architecture. We have developed a system that is capable of providing both GLAO and MOAO correction across the maximum possible field of view of the ELT, whilst minimizing system complexity and cost. When operating in ‘High-Definition Mode’ we expect to achieve >25% H-band ensquared energy within 160 milli-arcseconds in each of the 10 MOAO channels positioned anywhere within a 7.4 arcminute diameter field. For the ‘High-Multiplex’ modes (single objects) we expect to achieve a FWHM of 0.4” at 600nm, and 0.3” at 1600nm across the same field of view. These performance targets will be met with high sky coverage under at least median seeing conditions.

MOSAIC plans to start the preliminary design phase in early 2019.

#### ACKNOWLEDGMENTS

The authors would like to thank the wider MOSAIC consortium for the many discussions that have resulted in this work presented in this paper. This authors acknowledge the financial support from STFC grant number ST/M007669/1, Horizon 2020 funded GreenFlash project (Identification 671662 under FETHPC-1-2014), CNRS/INSU, Observatoire de Paris and the OPTICON project (EC FP7 grant agreement 312430).

#### REFERENCES

- [1] Jagourel, P. et al, “MOSAIC: the multi-object spectrograph of the ELT,” Proc. SPIE 10702, 10702- (2018)
- [2] Hammer, F., et al, “The ELT-MOS: towards the construction phase,” Proc. SPIE 10702, 10702- (2018)
- [3] Gratadour, D. et al, “Green Flash: Exploiting future and emerging computing technologies for AO RTC at ELT scale,” AO4ELT5 (2017)
- [4] Downing, M., et al, “AO WFS detector developments at ESO to prepare for the E-ELT,” Proc. SPIE 9909, 990914 (2016).
- [5] Gendron, E., “Optical solutions for accommodating ELT LGS wave-front sensing to small format detectors,” Proc. SPIE 9909, 99095Z (2016)
- [6] Bardou, L., et al, “Preliminary on-sky results of the CANARY experiment with an ELT-elongated sodium LGS”, AO4ELT5 (2017)

- [7] Basden, A.G. et al, "A modular design for the MOSAIC AO real-time control system," Proc. SPIE 10707, 10707-(2018).
- [8] Jenkins, D. R., et al, "An ELT scale MCAO real-time control prototype using Many Core technologies," Proc. SPIE 10703, 10703- (2018)
- [9] Doucet, N., et al, "Scalable soft-real time supervisor module for tomographic AO," Proc. SPIE 10703, 10703-(2018)
- [10] Basden, A.G. and Morris, T. J., "Monte Carlo modelling of multi-object adaptive optics performance on the European Extremely Large Telescope," MNRAS 463, 4184-4193 (2016)
- [11] Rousset, G., et al, "EAGLE MOAO system conceptual design and related technologies," Proc. SPIE 7736, 77360S (2010)
- [12] Cuby, J.-G., et al, "EAGLE: A MOAO-fed Multi-IFU workhorse for E-ELT," Proc. SPIE 7735, 77352D (2010)
- [13] Basden, A.G., Evans, C. J. and Morris, T.J., "Wide-field adaptive optics performance in cosmological deep fields for multi-object spectroscopy with the European Extremely Large Telescope," MNRAS 445, 4408-4014 (2014)
- [14] Morris, S.L., et al, "The EAGLE instrument for the E-ELT: developments since delivery of Phase A," Proc. SPIE 8446, 84461J (2012)
- [15] Morel, C., et al, "Pseudo-analytic simulation of woofer-tweeter MOAO system: application to MOSAIC," Proc. SPIE 9909, 990976 (2016)
- [16] Morris, T., et al, "Adaptive optics for MOSAIC: design and performance of the wide(st)-field AO system for the E-ELT," Proc. SPIE 9909, 99091I (2016)
- [17] Martinez, P. et al, "On the Difference between Seeing and Image Quality: When the Turbulence Outer Scale Enters the Game," ESO Messenger 141, 5 (2010)
- [18] Neichel, B., Fusco, T., Conan, J.-M., "Tomographic reconstruction for Wide Field Adaptive Optic systems: Fourier domain analysis and fundamental limitations", J. Opt. Sci. Am. A, 26, 1, 219-235 (2009)